HHS Public Access

Author manuscript

Cell Rep. Author manuscript; available in PMC 2017 November 28.

Published in final edited form as:

Cell Rep. 2017 August 29; 20(9): 2262–2276. doi:10.1016/j.celrep.2017.08.027.

Genome-wide maps of m6A circRNAs identify widespread and cell-type-specific methylation patterns that are distinct from mRNAs

Chan Zhou[1,†], **Benoit Molinie**[1,†], **Kaveh Daneshvar**[1], **Joshua V. Pondick**[1], **Jinkai Wang**[2], **Nicholas O. Van Wittenberghe**[1], **Yi Xing**[2], **Cosmas C. Giallourakis**[1,3,*], and **Alan C. Mullen**[1,3,*,#]

[1]Gastrointestinal Unit, Massachusetts General Hospital, Harvard Medical School, Boston, Massachusetts 02114 USA

[2]Department of Microbiology, Immunology and Molecular Genetics, University of California, Los Angeles, Los Angeles, CA 90095, USA

[3]Harvard Stem Cell Institute, Cambridge, MA 02138 USA

Summary

N^6-methyladenosine (m^{6}A) is the most abundant internal modification of mRNAs and is implicated in all aspects of post-transcriptional RNA metabolism. However, little is known about m^{6}A modifications to circular (circ) RNAs. We developed a computational pipeline (AutoCirc) that together with depletion of ribosomal RNA and m^{6}A immunoprecipitation defined thousands of m^{6}A-circRNAs, with cell-type-specific expression. The presence of m^{6}A-circRNAs is corroborated by interaction between circRNAs and YTHDF1/YTHDF2, proteins that read m^{6}A sites in mRNAs, and by reduced m^{6}A levels upon depletion of METTL3, the m^{6}A writer. Despite sharing m^{6}A readers and writers, m^{6}A-circRNAs are frequently derived from exons that are not methylated in mRNAs, while mRNAs that are methylated on the same exons that compose m^{6}A-circRNAs exhibit less stability, in a process regulated by YTHDF2. These results expand our understanding of the breadth of m^{6}A modifications and uncover regulation of circRNAs through m^{6}A modification.

Keywords

circular RNAs; m6A modification; noncoding RNAs; embryonic stem cells; METTL3; YTHDF2

*Corresponding authors: cgiallourakis@mgh.harvard.edu acmullen@mgh.harvard.edu.
†These authors contributed equally to this work
#Lead author: acmullen@mgh.harvard.edu

Supplemental Information

Supplemental information includes Extended Experimental Procedures, seven supplemental figures and four supplemental tables.

Author Contributions

C.C.G. and A.C.M. conceived the study. C.C.G. and A.C.M. designed experiments with C.Z., B.M. and K.D. Computational analyses were performed by C.Z. with support from J.V.P., J.W. and Y.X. Bench experiments were performed by B.M. and K.D. with assistance from J.V.P and N.O.V.W. The manuscript was written by C.Z., C.C.G. and A.C.M. with input from B.M.

Introduction

N6-methyladenosine (m^6A) was the first identified mammalian internal messenger (m) RNA modification and remains the most abundant modification known on mRNAs and long noncoding (lnc) RNAs (Gilbert and Bell, 2016). A renewed interest in RNA modifications catalyzed by technological advances has revealed the widespread nature of m^6A in eukaryotic cells from yeast to humans as well as its reversibility in mammalian cells (Dominissini et al., 2012; Jia et al., 2013; Meyer et al., 2012; Schwartz et al., 2013). The identification of proteins that act as "writers," "readers," and "erasers" of m^6A, as well as recognition of other internal modifications such as 5-methylcytosine (Squires et al., 2012), N1-methyladenosine (Ozanick et al., 2005), and pseudouridine (Staehelin, 1971) have led to the field coined 'epitranscriptomics'. m^6A has been implicated in all aspects of post-transcriptional RNA metabolism including half-life, splicing, translational efficiency, nuclear export, and RNA structure (Lichinchi et al., 2006; Spitale et al., 2015; Wang et al., 2014, 2015).

The development of m^6A location analyses utilizing anti-m^6A antibodies coupled to RNA-sequencing after RNA fragmentation has revealed sites of m^6A modifications located on thousands of mRNAs and hundreds of lncRNAs in numerous primary and transformed cells (Chen et al., 2015; Linder et al., 2015). Along with site and cell/tissue specificity, m^6A modifications exhibit global enrichment in the 3′UTR near mRNA stop-codons and long internal exons, leading to unique m^6A-derived transcriptome topology (Batista et al., 2014; Dominissini et al., 2012; Ke et al., 2015; Meyer et al., 2012). The writing of m^6A is accomplished via an m^6A methyltransferase complex composed of a core METTL3 and METTL14 heterodimer (Liu et al., 2014; Wang et al., 2016a, 2016b), and depletion of either METTL3 or METTL14 decreases m^6A levels in mRNAs to a similar degree (Liu et al., 2014; Ping et al., 2014). Proteins containing the YTH domain directly bind m^6A sites and act as readers of the m^6A signal (Wang et al., 2014, 2015; Xiao et al., 2016). YTHDF2 proteins recruit m^6A-modified mRNAs to nuclear p-bodies, promoting RNA degradation (Wang et al., 2014), while YTHDF1 promotes the translation of m^6A-modified mRNAs through interaction with translation initiation machinery (Wang et al., 2015).

We asked how broadly the concept of an epitranscriptome extends from linear RNAs to circRNAs, which are created by the covalent linkage of the 3′ and 5′ ends of spliced RNA transcripts resulting in circularization (Salzman et al., 2012). These back splice events were initially described in mammalian cells as a source of scrambled exons (Nigro et al., 1991) before they were linked to circRNAs (Capel et al., 1993). Nearly two decades later, high-throughput sequencing of total RNAs depleted of ribosomal (r) RNAs revealed the abundance of circRNAs (Salzman et al., 2012). Subsequent studies suggested that circRNAs can interact with transcriptional machinery, cyclin-dependent kinases, and microRNAs (Du et al., 2016; Hansen et al., 2013; Memczak et al., 2013; Zhang et al., 2013) and are potential biomarkers for disease (Shang et al., 2016; Xuan et al., 2016). However, the extent to which circRNAs are marked by the same m^6A modification found in mRNAs and lncRNAs is unclear.

Here we identify more than one thousand m^{6}A-circRNAs in human embryonic stem cells (hESCs) and show that m^{6}A-circRNAs are also abundant in HeLa cells. Comparison of m6A-circRNA maps between hESCs and HeLa cells reveals both common and cell-type-specific m^{6}A-circRNA expression patterns. Surprisingly, a large percentage of m^{6}A-circRNAs do not overlap with exons containing m^{6}A peaks in mRNAs in both cell types. The m^{6}A readers YTHDF1 and YTHDF2 interact with m^{6}A-circRNAs, and the m^{6}A writer METTL3 regulates m^{6}A levels, suggesting that much of the same cellular machinery is shared between m^{6}A modified circRNAs and mRNAs. Our analyses also uncovered an unexpected connection between m^{6}A-circRNAs and mRNA half-life regulated by YTHDF2. These results expand our understanding of the breadth and regulatory aspects of m^{6}A modifications through identification of the circRNA epitranscriptome.

Results

RNase R Resistant RNA Species are Modified by m^{6}A

m^{6}A modifications have been described in mRNAs and lncRNAs, and we wanted to determine if circRNAs may also be modified by m^{6}A. We analyzed three fractions of hESC RNA for the presence of m^{6}A modifications by anti-m^{6}A dot blot after rRNA depletion and RNAse R digestion to degrade linear RNAs (Suzuki et al., 2006) (Figure 1). Bioanalyzer analysis was also performed to evaluate the RNA at each step in this process (Figure S1A). The input RNA (rRNA-depleted, RNAse R-treated) and eluate fraction (m^{6}A-positive fraction following m^{6}A RNA immunoprecipitation (RIP)) both contain m^{6}A modifications, while the supernatant (m^{6}A-negative fraction) shows no evidence of m^{6}A (Figure 1A *bottom*). It is unlikely that the positive signal in the eluate fraction is due to tRNAs, which are also resistant to RNase R, because tRNAs are not modified by m^{6}A in mammalian cells (Mishima et al., 2015). This conclusion is supported by the loss of the RNA peak around 75 nucleotides (nt) following m^{6}A RIP (Figure S1A, eluate), which contains tRNAs (Holley et al., 1965). These results show that RNase R-resistant (nonlinear) RNAs contain a strong m^{6}A signal, and suggest that circRNAs contained in this pool may be modified by m^{6}A.

METTL3 and METTL14 are Required for m^{6}A Modifications of Non-linear RNAs

METTL3 and METTL14 physically interact in a synergistic complex, which is required for m^{6}A modification of polyadenylated (polyA) RNAs (Liu et al., 2014), and we asked if METTL3 and/or METTL14 are also required for m^{6}A modification of non-linear RNAs. Depletion of *METTL3* and/or *METTL14* by small interfering (si) RNAs in HEK-293T cells (Figure 1B and S1B) resulted in reduced m^{6}A methylation of polyA RNAs as expected (Figure 1C, **top and** S1C, top) (Batista et al., 2014; Liu et al., 2014). Analysis of rRNA-depleted and RNase R-digested RNA after depletion of *METTL3* or *METTL14* also demonstrated a reduction in m^{6}A modification of non-linear (circRNA-enriched) RNA compared to negative controls, and this reduction was more pronounced upon combined *METTL3/14* depletion. (Figure 1C, **bottom and** S1C, bottom). Together, these data show that there is an RNase R-resistant fraction of RNA that is dependent on METTL3/14 for m^{6}A modification and suggest that circRNAs may be modified by the METTL3/14 complex.

Computational Pipeline to Identify CircRNAs

To test for the existence of m^{6}A-modified circRNAs, we developed a computational pipeline (AutoCirc) to identify back splice junctions characteristic of circRNAs (Figure 2A, see Materials and Methods). AutoCirc identified 2,679 total circRNAs by the presence of at least two unique reads spanning a back splice in the union of biological replicates. We validated the presence of back splice junctions identified by AutoCirc with reverse transcription (RT)-PCR (Figure 2B) and Sanger sequencing (Figure 2C). The analyzed circRNAs were chosen to include examples from the most abundant (encoded by *SMO*), moderately abundant (encoded by *SLC11A2*), and least abundant (encoded by *FO XK2*) groups of circRNAs based on back splice counts (Supplemental Table S1).

We then compared AutoCirc to CIRCexplorer and MapSplice, which have performed well in other studies (Hansen et al., 2015; Zhang et al., 2014). All three pipelines identify similar populations of circRNAs (2,679 by AutoCirc, 2,425 by CIRCexplorer and 2,704 by MapSplice) using a threshold of two unique reads spanning a back splice junction in our rRNA-depleted hESC RNA samples. Approximately 80% of the back splice junctions identified by CIRCexplorer were also identified by AutoCirc. The circRNAs identified by AutoCirc or CIRCexplorer each have a slightly smaller degree of overlap with the circRNAs identified by MapSplice than they do with each other (Figure S2A). 887 back splice junctions identified by MapSplice are unique compared to 254 for CIRCexplorer and 479 for AutoCirc. The increased number of unique back splice junctions identified by MapSplice is likely due to the use of the ENCODE gene annotation by MapSplice compared to RefSeq for CIRCexplorer and AutoCirc, as the ENCODE annotation contains a larger number of genes. As a negative control for circRNA detection, we analyzed polyA RNA from hESCs (Sigova et al., 2013), and all three pipelines identified a similar low frequency of back splice junctions (Figure S2B). AutoCirc is about 10 fold faster than CIRCexplorer and about 250 fold faster than MapSplice and consumes fewer computing resources (memory threads and number of processes) (Supplemental Table S2).

Identification of m^{6}A-circRNAs in hESCs

To test for the existence of m^{6}A-modified circRNAs in hESCs, we prepared libraries for RNA sequencing after rRNA depletion (input) followed by m^{6}A RIP (eluate) (Figure S2C). To confirm the specificity of the m^{6}A RIP, we added exogenous RNA spike-ins with and without m^{6}A modifications to each RNA sample after rRNA-depletion. Only spike-ins containing m^{6}A-modified RNAs were detected after m^{6}A RIP (Figure S2D), consistent with our previous experience (Batista et al., 2014; Molinie et al., 2016).

We applied AutoCirc after m^{6}A RIP and identified 1,404 m^{6}A-circRNAs (Figure 2D). Fifty-four percent of m^{6}A-circRNAs were contained in the pool of total circRNAs (Figure S2E), and this increased to 83% when we expanded the pool of total circRNAs by including additional hESC data sets (Figure S2F). We quantified expression of m^{6}A-circRNAs verses those predicted not to be methylated by their presence in the input and absence in m^{6}A RIP samples. We performed these experiments before and after depletion of *METTL3* to assess for the requirement of METTL3 for m^{6}A modifications in circRNAs (Figure 2E). m^{6}A-circRNAs encoded by *FAT3, HIPK3*, and *SLC45A4* were chosen due to their high

abundance, and the m^{6}A-circRNA encoded by *NUFIP2* was chosen as an example of an m^{6}A-circRNA with lower abundance (Supplemental Table S1). Black bars represent samples without depletion of *METTL3* and show enrichment of m^{6}A-circRNAs (encoded by *FAT3*, *HI PK3*, *SLC45A4,* and *NUFIP2*) after m^{6}A RIP compared to non-m^{6}A-circRNAs (encoded by *SMO*, *SLC11A2*, and *FOXK2*) (Figure 2E, *right*). Dark and light gray shading represent two independent siRNAs used to deplete *METTL3* (Figure 2E, *left*). Depletion of *METTL3* did not affect the total expression levels of circRNAs regardless of whether they were identified as m^{6}A-circRNAs or non-m^{6}A-circRNAs (Figure S2G). However, depletion of *METTL3*, was associated with a decrease in the level of m^{6}A-circRNAs (Figure 2E, *right*), suggesting that METTL3 regulates m^{6}A modification in circRNAs. The back splices that define each m^{6}A-circRNA were confirmed by Sanger sequencing, and RNA-seq tracks show enrichment of the exons encoding circRNAs following m^{6}A RIP (Figure 2F, S2H). These results establish a transcriptome-wide map of m^{6}A-circRNAs in hESCs.

m^{6}A Methylation is Enriched in CircRNAs Composed of Long Single Exons

We next evaluated the features of m^{6}A-circRNAs and non-m^{6}A-circRNAs. We sequenced the m^{6}A-depleted RNA (supernatant from m^{6}A RIP) and applied AutoCirc (Figure 2A) to provide more stringent criteria to define the population of circRNAs enriched in non-m^{6}A-circRNAs. We examined the distributions of genomic origins of total circRNAs identified from input, m^{6}A-circRNAs identified from eluate, and non-m^{6}A-circRNAs from supernatant. m^{6}A-circRNAs and non-m^{6}A-circRNAs show a similar genomic distribution; approximately 80% of circRNAs from both categories are derived from exons of protein-coding genes (Figure 3A). Parent genes for both m^{6}A-circRNAs and non-m^{6}A-circRNAs are also similarly enriched in the gene ontogeny (GO) categories of enzyme binding and transcription factor activities (Figure S3A). The majority of total circRNAs that originate from protein-coding genes span two or three exons (Figure 3B, *left*), whereas m^{6}A-circRNAs are more commonly encoded by single exons compared to non-m^{6}A-circRNAs (Figure 3B, *right*). The exons of single exon circRNAs tend to be longer than the exons of multi-exon circRNAs for all groups of circRNAs (Figure 3C). Furthermore, the lengths of all exons in m^{6}A-circRNAs tend to be longer than those in non-m^{6}A-circRNAs (Figure 3D). Single exon circRNAs are also more abundant than multiple-exon circRNAs in m^{6}A-circRNAs compared to non-m^{6}A-circRNAs ($p<1.2e-9$ in m^{6}A-circRNAs vs $p=0.52$ in non-m6A-circRNAs, Figure 3E). Thus, m^{6}A methylation is enriched in circRNAs composed of long single exons, which are more abundant than multi-exon m^{6}A-circRNAs.

m^{6}A-circRNAs Exhibit Distinct Patterns of m^{6}A Modifications Compared to mRNAs

m^{6}A sites in mRNAs are most common in the last exon (Meyer et al., 2012); however, circularization of the last exon of genes is uncommon (Zhang et al., 2014). We found that 73% of parent genes of m^{6}A-circRNAs also encode m^{6}A-mRNAs in hESCs (Figure 4A). We then examined if exons methylated in mRNAs are the same exons that form m^{6}A-circRNAs. Surprisingly, the majority (59%) of m^{6}A-circRNAs were produced from exons without m^{6}A peaks in mRNAs (Figure 4B). Thirty-three percent of m^{6}A-circRNAs were produced from genes that encode m^{6}A-mRNAs methylated on different exons, and 26% of m^{6}A-circRNAs were produced from genes that encode mRNAs without detectable m^{6}A modification. This observation is also reflected in the different distributions of m^{6}A-circRNAs and m^{6}A peaks

in mRNAs across genes (Figure 4C). These results suggest a different set of rules may govern m^{6}A biogenesis in circRNAs.

We performed qRT-PCR on fragmented, polyA-selected RNA before and after m^{6}A RIP to confirm the m^{6}A status of linear transcripts that also encode circRNAs. The first category represents genes including *METTL3 and ZNF398* that encode m^{6}A-circRNAs from exons that also have an m^{6}A peak in mRNAs. We confirmed the presence of m^{6}A-circRNAs encoded by *METTL3* and *ZNF398* by RT-PCR (Figure S4A). Primers were designed to detect the m^{6}A mRNA peak within the exons encoding the m^{6}A-circRNA (primers P1) and to detect a region of the mRNA without m^{6}A enrichment (primers P2) (Figures 4D, **top and** S4B, top). After m^{6}A RIP, we detected amplification with P1 but not P2 primers (Figures 4E **and** S4C, top-left). P1 and P2 primers both amplified fragmented mRNA confirming the presence of both exons in polyA-selected RNA (Figures 4E **and** S4C, top-right). The second category of genes, including *SO X13* and *ARHG EF19,* encode m^{6}A-circRNAs from exons different from those containing m^{6}A peaks in mRNAs. Primers P1 amplify RNA from exons encoding the m^{6}A-circRNA, and primers P2 amplify the m^{6}A-mRNA peak defined by sequencing (Figures 4D **and** S4B, middle). After m^{6}A RIP, we detected amplification of with P2 but not P1 primers, consistent with different sites of m^{6}A modifications between m^{6}A circRNAs and m^{6}A mRNAs encoded by the same genes. (Figures 4E **and** S4C, middle). Both primer sets amplified mRNA before m^{6}A RIP (Figures 4E **and** S4C, middle-right). The third category of genes, including *G FM2* and *MAPKAP1*, encode m^{6}A-circRNAs from genes that do not encode m^{6}A mRNAs. We did not detect m^{6}A modifications in mRNAs within the exons encoding m^{6}A-circRNAs (P1) or other regions (P2), (Figures 4D **and** S4B, bottom), but both primer sets amplified mRNA (Figures 4E **and** S4C, bottom). These results validate the finding that numerous m^{6}A-circRNAs are generated from exons that do not contain m^{6}A peaks in mRNAs.

CircRNAs Exhibit Unique Patterns of m^{6}A Methylation in Different Cell Types

To determine if m^{6}A modifications in hESCs were representative of mammalian cells in general, we repeated the sequencing analysis in HeLa cells. We identified 854 circRNAs from input (rRNA-depletion), 987 m^{6}A-circRNAs from eluate (rRNA-depletion, m^{6}A RIP), and 899 non-m^{6}A-circRNAs from supernatant after m^{6}A RIP (Figure S5A). The genomic distribution, exon length, and number of exons in m^{6}A-circRNAs and non-m^{6}A-circRNAs are similar between hESCs and HeLa cells (Figures S5A–C). Similar to m^{6}A-circRNAs in hESCs, half of the m^{6}A-circRNAs identified in HeLa cells originate from exons that do not contain the m^{6}A modification in mRNAs (Figure S5D).

More than half of the m^{6}A-circRNAs detected in HeLa cells were not detected in hESCs (Figure S5E), suggesting that many m^{6}A-circRNAs are uniquely expressed in the two cell types. HeLa cells and hESCs do not express all of the same genes or circRNAs, so we asked if the differences in m^{6}A-circRNAs between HeLa cells and hESCs could be explained by differences in gene or circRNA expression. Sixty-five percent of m^{6}A-circRNAs detected in HeLa cells were not detected in hESCs even when the parent genes of these circRNAs are expressed in both cell types (Figure 5A**, top**). Furthermore, 41% of m^{6}A-circRNAs detected in HeLa cells were not detected in hESCs even when circRNAs are expressed in both cell

types (Figure 5A**, bottom**). HeLa cells and hESCs produce circRNAs from a small number of parent genes that do not express detectable mRNAs, which explains why there are more common m^{6}A-circRNAs between HeLa cells and hESCs among the shared circRNAs group (Figure 5A, *bottom*) compared to the shared parent genes group (Figure 5A, *top*). When m^{6}A-circRNAs are expressed in both cell types, they tend to be expressed at similar levels (Figure 5B and S5F).

RT-PCR confirmed that unique m^{6}A-circRNAs could be detected in the two different cell types. *RASSF8* and *KANK1* are expressed in both HeLa cells and hESCs, yet circRNAs from these two genes are detected only in HeLa cells, where they are m^{6}A-modified (Figure 5C, 5D**, top and** S5G, S5H, top). In contrast, *SEC11A* and *TMEFF1* are expressed in both HeLa cells and hESCs, but circRNAs are only detected in hESCs, where they are m^{6}A-modified (Figure 5C, 5D**, center and** S5G, S5H, center). CircRNAs encoded by *KIF20B* and *NUFIP2* are detected in both HeLa cells and hESCs and are both modified by m^{6}A based on m^{6}A RIP seq (Figure 5C, 5D, **bottom and** S5G, S5H bottom). Sanger sequencing confirmed the predicted back splice junctions for circRNAs encoded by *RASSF8*, *SEC11A*, and *NUFIP2* (Figure 5E). Furthermore, circRNAs encoded by *RAPGEF1* and *ATP5C1* are detected in both HeLa cells and hESCs, but are only detected after m^{6}A RIP in HeLa cells (Figure 5F, *left*) and hESCs (Figure 5F, *right*), respectively. These results show that many m^{6}A-circRNAs are expressed in a cell-type-specific manner.

m^{6}A-circRNA Levels

We next evaluated m^{6}A levels in circRNAs in HeLa cells and hESCs. We quantified the m^{6}A level for each circRNA by RNA abundance, defined as eluate/(eluate+supernatant) where eluate and supernatant samples were normalized using synthetic ERCC control RNAs (Molinie et al., 2016) (Figure S6A). The median methylation levels of circRNAs are reduced in hESCs compared to HeLa cells (Figure 6A) due to an enrichment of unmethylated or lowly methylated circRNAs in hESCs compared to HeLa cells (Figure 6B). Because the majority of unmethylated or lowly methylated circRNAs are only detected in supernatant samples, we also measured the distribution of m^{6}A levels for circRNAs detected in both eluate and supernatant. These circRNAs follow an almost bimodal distribution where most circRNAs exhibit less than 50% methylation (Figure S6B), similar to the distribution observed in mRNAs (Molinie et al., 2016). The overall m^{6}A-levels in circRNAs are higher in hESCs than in HeLa cells when restricting analysis to circRNAs detectable in both eluate and supernatant (Figure 6C). These results show that there are variable levels of m^{6}A-modification across circRNA species in a distribution similar to mRNAs.

m^{6}A Levels and CircRNA Expression

m^{6}A promotes mRNA degradation (Wang et al., 2014), and m^{6}A levels are inversely correlated with steady-state mRNA expression levels (Molinie et al., 2016). We asked how m^{6}A-levels are related to expression levels of circRNAs. In HeLa cells, m^{6}A-levels in circRNAs are positively correlated with the expression levels of circRNAs (Spearman correlation rho=0.41, p<2.2e-16), and in hESCs, m^{6}A-levels in circRNAs are positively correlated with the expression levels of circRNAs with m^{6}A levels > 0.3 (Spearman correlation rho=0.65, p<2.2e-16, Figure 6D). We did observe a negative correlation with

circRNA expression for low m^{6}A levels (<0.3) in hESCs (Spearman correlation rho= - 0.62, p<2.2e-16). These results suggest that at low levels of m^{6}A-modification, an increase in m^{6}A level can be associated with reduced circRNA expression in some conditions, but at m^{6}A levels over 0.3, increasing levels of m^{6}A-modification is not linked to decreased circRNA expression.

Transposable Elements are Enriched in the Flanking Regions of m^{6}A-circRNAs

Reverse complementary sequence in transposable elements (TEs) in the flanking regions of circRNAs promote the formation of circRNAs (Ashwal-Fluss et al., 2014; Chen et al., 2017; Liang and Wilusz, 2014; Zhang et al., 2014). We asked if there were characteristics of TEs in the flanking regions of circRNAs that are associated with m^{6}A modification. We found that TEs are significantly enriched in both the 5′ and 3′ flanking regions of m^{6}A-circRNAs (eluate) compared to circRNA pools depleted of m^{6}A (supernatant). The population of m^{6}A-circRNAs changes between cell types (Figure 5A and B), so we also analyzed the density of flanking TEs in the group of circRNAs that do not have evidence of m^{6}A modification in either HeLa cells or hESCs. These circRNAs have the lowest density of flanking TEs (Figure 6E). These results suggest that the density of TEs flanking circRNAs may be linked to formation of m^{6}A-circRNAs.

m^{6}A-circRNAs are recognized by YTHDF1 and YTHDF2

YTH-domain family member 1 (YTHDF1) recognizes m^{6}A-mRNAs and promotes translation (Wang et al., 2015), while YTHDF2 forms a complex with m^{6}A-mRNAs to target RNAs to decay sites (Wang et al., 2014). We asked if the YTH domain that recognizes m^{6}A-mRNAs also recognizes m^{6}A-circRNAs. We re-analyzed YTHDF1 and YTHDF2 RIP-seq data (Wang et al., 2014, 2015) using AutoCirc (Figure 2A) to identify circRNAs bound by YTHDF1 and YTHDF2 (Figure 7A). We identified 1,155 circRNAs interacting with YTHDF1 and 1,348 circRNAs interacting with YTHDF2 (Figure 7B). These circRNAs show a similar distribution across the genome to that of m^{6}A-circRNAs (Figure 7B **and** Figure S5A) and are generated from the same categories of genes by GO analysis (Figure S7A). In addition, the circRNAs that interact with YTHDF1 and YTHDF2 are formed primarily from exons immediately downstream of the start of coding regions (Figure 7C). Twenty-eight percent and 22% of the YTHDF1 and YTHDF2 bound circRNAs, respectively, were also identified as m^{6}A-circRNAs in HeLa cells (Figure 7D), and 51% of circRNAs interacting with YTHDF1 also interact with YTHDF2 (Figure S7B). To evaluate the possibility that circRNAs may interact with proteins independent of m^{6}A modifications, we analyzed RIP-seq data for AGO2 (Polioudakis et al., 2015), a protein which is not known to bind m^{6}A. Analyses are normalized to sequencing depth, and show that YTHDF1 and YTHDF2-bound circRNAs are significantly enriched in m^{6}A-circRNAs compared to AGO2-bound circRNAs (p<0.0041) (Figure 7E).

m^{6}A-circRNAs are Linked to mRNA Stability by YTHDF2

YTHDF2 interacts with m^{6}A-mRNAs to regulate mRNA stability (Wang et al., 2014), and mRNAs encoded by the parent genes of m^{6}A-circRNAs also have a shorter half-life than mRNAs encoded by the parent genes of non-m^{6}A-circRNAs (Figures 7F **and** S7C). This

finding is observed for m^{6}A-circRNAs identified by m^{6}A RIP or interaction with YTHDF1/YTHDF2, regardless of whether the mRNA contains an m^{6}A modification. We then performed the same analysis but separated m^{6}A negative (m^{6}A(−)) from m^{6}A positive (m^{6}A(+)) mRNAs (Figure 7G **and** S7D). This analysis showed that m^{6}A-mRNAs encoded by the parent genes of m^{6}A-circRNAs are the only group with significantly reduced half-lives compared to genes not encoding any circRNAs. These results suggest that in addition to the m^{6}A modification of mRNAs being associated with a shorter mRNA half-life (Wang et al., 2014), those m^{6}A-mRNAs encoded by the parent genes of m^{6}A-circRNAs have shorter half-lives among all m^{6}A-mRNAs. Genes encoding both m^{6}A-mRNAs and m^{6}A-circRNAs can produce these transcripts from the same (Figure 7H, **diagram A**) or different exons (**diagram B**). The m^{6}A-mRNAs with the shortest half-lives are those in which m^{6}A-circRNAs are produced from the same exons that have m^{6}A modifications in mRNAs (Figure 7H **and** S7E). m^{6}A is most commonly enriched in the 3′ UTR of mRNAs (Batista et al., 2014; Dominissini et al., 2012; Ke et al., 2015; Meyer et al., 2012), while circRNAs are enriched in the gene body (Figure 4C and 7C). We examined if differences in the location of the m^{6}A modification in mRNAs could explain the difference in half-lives and found no significant difference in the half-lives of m^{6}A-mRNAs that are modified in the gene body or 3′ UTR (Figure S7F). Finally, the half-lives of m^{6}A-mRNAs that are methylated in the same exons that are methylated in circRNAs increase with depletion of YTHDF2 (Figures 7I **and** S7G), suggesting that stability of this subset of RNAs is controlled by YTHDF2 in a process that may involve recognition of m^{6}A-circRNAs.

Discussion

This study brings together two rapidly expanding fields: RNA modifications and circRNAs. Here, we present transcriptome-wide identification of m^{6}A-circRNAs, extending the concept of the RNA epitranscriptome to circRNAs. We provide evidence that m^{6}A modifications in circRNAs are written and read by the same machinery (METTL3/14, YTH proteins) used for mRNAs, but often at different locations. We implicate m^{6}A-circRNAs in mRNA stability mediated by YTHDF2, but m^{6}A does not appear to promote degradation of circRNAs as it does for mRNAs. Furthermore, we identify many m^{6}A-circRNAs expressed in a cell-type-specific pattern even when their parental genes (or circRNAs) are expressed in both cell types, suggesting that the m^{6}A modification of circRNAs may regulate different biological processes in different cell types. Our results establish a fertile area of investigation to define the breadth and function of covalent modifications in circRNAs.

The discovery of m^{6}A-circRNAs raises many questions that will need to be addressed in future studies, including the significance of m^{6}A-modifications on exons that compose circRNAs but are not modified in mRNAs. Nevertheless, our results show that identification of m^{6}A-circRNA patterns may be useful to identify different cell types/states even in the absence of significant changes in baseline mRNA expression, leading to methodologies to fingerprint cells. Furthermore, it will be of interest to address whether m^{6}A-circRNAs are found in extracellular vesicles, which have been proposed as a mechanism to clear circRNAs from cells (Lasda and Parker, 2016).

In terms of m^{6}A-circRNA functionality, we provide evidence of cross-talk between m^{6}A-modified mRNAs and circRNAs that affects mRNA half-life in a YTHDF2-dependent manner. However, it is unclear if recognition of m^{6}A-circRNAs by YTHDF2 plays a direct role. One potential model is that m^{6}A-circRNAs and m^{6}A-mRNAs encoded by the same exons are bundled as part of a chromatin-associated liquid phase transition leading to a nuclear "liquid droplet" (Caudron-Herger et al., 2016; Marzahn et al., 2016) and continue to be a topologically and organizationally distinct information packets. Whereas m^{6}A-circRNAs arising from non-methylated exons of mRNAs may not be bundled with mRNAs or are contained in other bundles. It is possible that these information packet(s) are transmitted to the cytosol leading to differential mRNA processing via interaction with cytosolic liquid droplets, that may include m^{6}A binding to YTH domain proteins, which harbor poly Q unstructured domains (Guo and Shorter, 2015; Wang et al., 2014; Zhang et al., 2015). We postulate that circRNAs in general may exhibit unique tuning qualities on liquid droplets, affecting surface tension, stability, size and/or longevity. m^{6}A-circRNAs may further modify these characteristics given their ability to interact with YTH proteins as well as other RNA binding proteins (Guo and Shorter, 2015; Lin et al., 2015).

Controlling the state of m^{6}A modifications in circRNAs may act as switches to control circRNA functionality. For example, the presence of m^{6}A modifications can promote the translation of m^{6}A-circRNAs (Yang et al., 2017). This study focused on m^{6}A modifications located near back splice junctions, which were identified by sequencing circRNAs that underwent m^{6}A RIP after fragmentation. This approach yielded fewer circRNAs compared to our analysis because we performed m^{6}A RIP on un-fragmented circRNAs to identify the abundance of m^{6}A-circRNAs. CircRNAs can also be engineered to be translatable with internal ribosome entry sites (Chen and Sarnow, 1995; Wang and Wang, 2015), and a few circRNAs are found to be translated into peptides in a splice-dependent/cap-independent manner (Legnini et al., 2017; Pamudurti et al., 2017). m^{6}A modification is also implicated in the splicing of mRNAs (Liu et al., 2015), and m^{6}A modification could be involved in alternative splicing of some circRNAs.

Many m^{6}A-circRNAs originate from exons where m^{6}A modifications are absent on mRNAs, indicating that while the writing and reading machinery of m^{6}A modifications are similar in both mRNAs and circRNAs, different patterns of m^{6}A modifications are produced in different types of RNA. How do we reconcile the presence of m^{6}A-circRNAs arising from exons that are non-methylated in polyA-selected mRNA species? The locations of m^{6}A modifications in nascent pre-mRNAs and mRNAs are highly conserved, suggesting that m^{6}A modifications in mRNAs occur by the time nascent pre-mRNA is formed (Ke et al., 2017). These conclusions, together with our findings that m^{6}A-circRNAs are frequently modified in exons that are not m^{6}A-modified in mRNAs suggest that some m^{6}A modifications to circRNAs may occur during or after circRNA formation. TEs are present in the flanking regions of circRNAs to facilitate the formation of stem loops during back splicing events (Ashwal-Fluss et al., 2014; Liang and Wilusz, 2014; Zhang et al., 2014), METTL3/14 have been shown to bind TEs (Kelley et al., 2014), and TEs are enriched in the flanking regions of m^{6}A-circRNAs compared to non-m^{6}A-circRNAs (Figure 6E). These findings support a model in which methylation of some circRNAs is linked to circRNA formation.

Experimental Procedures

RNA isolation, m^{6}A immunoprecipitation, and library preparation

Total RNA was obtained by TRIzol extraction followed by DNAse I treatment prior to rRNA depletion. RNase R treatment (5 units per μg RNA) was performed in duplicate with 5 μg of rRNA-depleted RNA input. m^{6}A RIP was performed using an anti-m^{6}A antibody (Synaptic Systems # 202 003). PolyA RNA selection was performed twice using the Dynabeads mRNA Purification Kit with 7.5 μg of total RNA input. 100 ng of RNA was used for library construction.

Computational pipeline for detecting circRNAs

We performed directional, 100 × 100 paired-end sequencing to define circRNAs. Paired reads were treated independently and mapped to the human reference genome (hg19). We used Bowtie2 (Langmead and Salzberg, 2012) to identify and discard all sequences that mapped to a contiguous region of genomic DNA. We developed AutoCirc to scan 20 nucleotides at both ends of each 100 nt sequence of unmapped reads to identify sequences that contain back splice junctions of circRNAs (see Supplemental Materials and Methods for details). AutoCirc is available at https://github.com/chanzhou/AutoCirc.

Identification of circRNAs interacting with YTHDF1, YTHDF2, and AGO2

We applied the AutoCirc pipeline to identify circRNAs from YTHDF1 (GSE63591), YTHDF2 (GSE49339) and AGO2 RIP (GSE64615) in HeLa cells. We counted the circRNAs with a single read or greater as present in a replicate as long as there were at least two reads supporting a specific back splice in the union of all replicates.

Evaluation of mRNA half-life

We obtained mRNA half-life data from siControl and siYTHDF2 in HeLa cells (Wang et al., 2014). We separated the mRNAs into groups as described. mRNAs produced by genes that did not produce circRNAs were used as a control group. To examine how the interaction between YTHDF2 and m^{6}A-circRNAs affects m^{6}A-mRNA half-life, we plotted the accumulation fraction curve of the log2-transformed changed half-life between siYTHDF2 and siControl cells for m^{6}A-mRNAs methylated in the same exons as m^{6}A-circRNAs and m^{6}A-mRNAs methylated in different exons from m^{6}A-circRNAs encoded by the same gene.

Data access

The accession number for RNA-seq data produced for this study is GEO: GSE85324.

Supplementary Material

Refer to Web version on PubMed Central for supplementary material.

Acknowledgments

We would like to thank P. Dedon and K. Jeffrey for helpful discussions, X. Zhao for suggestions on pipeline implementation, and the MGH Sequencing core and Tufts University Genomics core for RNA sequencing. This work was supported National Institutes of Health (NIH) grant R01GM088342, an Eli & Edythe Broad Center of

Regenerative Medicine and Stem Cell Research at UCLA and Rose Hills Foundation Research Award, and an Alfred Sloan Research Fellowship (Y.X.). This work was also supported by Massachusetts General Hospital start-up funds (C.C.G. and A.C.M.).

References

Ashwal-Fluss R, Meyer M, Pamudurti NR, Ivanov A, Bartok O, Hanan M, Evantal N, Memczak S, Rajewsky N, Kadener S. circRNA Biogenesis Competes with Pre-mRNA Splicing. Mol Cell. 2014:1–12.

Batista PJ, Molinie B, Wang J, Qu K, Zhang J, Li L, Bouley DM, Lujan E, Haddad B, Daneshvar K, et al. m6A RNA Modification Controls Cell Fate Transition in Mammalian Embryonic Stem Cells. Cell Stem Cell. 2014; 15:707–719. [PubMed: 25456834]

Capel B, Swain a, Nicolis S, Hacker a, Walter M, Koopman P, Goodfellow P, Lovell-Badge R. Circular transcripts of the testis-determining gene Sry in adult mouse testis. Cell. 1993; 73:1019–1030. [PubMed: 7684656]

Caudron-Herger M, Pankert T, Rippe K. Regulation of nucleolus assembly by non-coding RNA polymerase II transcripts. Nucleus. 2016; 7:308–318. [PubMed: 27416361]

Chen CY, Sarnow P. Initiation of protein synthesis by the eukaryotic translational apparatus on circular RNAs. Science. 1995; 268:415–417. [PubMed: 7536344]

Chen K, Lu Z, Wang X, Fu Y, Luo GZ, Liu N, Han D, Dominissini D, Dai Q, Pan T, et al. High-resolution N6-methyladenosine (m6A) map using photo-crosslinking-assisted m6A sequencing. Angew Chemie - Int Ed. 2015; 54:1587–1590.

Chen L, Zhang P, Fan Y, Huang J, Lu Q, Li Q, Yan J. Transposons modulate transcriptomic and phenotypic variation via the formation of circular RNAs in maize. 2017

Dominissini D, Moshitch-Moshkovitz S, Schwartz S, Salmon-Divon M, Ungar L, Osenberg S, Cesarkas K, Jacob-Hirsch J, Amariglio N, Kupiec M, et al. Topology of the human and mouse m6A RNA methylomes revealed by m6A-seq. Nature. 2012; 485:201–206. [PubMed: 22575960]

Du WW, Yang W, Liu E, Yang Z, Dhaliwal P, Yang BB. Foxo3 circular RNA retards cell cycle progression via forming ternary complexes with p21 and CDK2. Nucleic Acids Res. 2016; 44:2846–2858. [PubMed: 26861625]

Gilbert WV, Bell TA. Messenger RNA modifications: Form, distribution, and function. Science. 2016; 352

Guo L, Shorter J. It's Raining Liquids: RNA Tunes Viscoelasticity and Dynamics of Membraneless Organelles. Mol Cell. 2015; 60:189–192. [PubMed: 26474062]

Hansen TB, Jensen TI, Clausen BH, Bramsen JB, Finsen B, Damgaard CK, Kjems J. Natural RNA circles function as efficient microRNA sponges. Nature. 2013; 495:384–388. [PubMed: 23446346]

Hansen TB, Venø MT, Damgaard CK, Kjems J. Comparison of circular RNA prediction tools. Nucleic Acids Res. 2015; 44:1–8. [PubMed: 26621913]

Holley RW, Apgar J, Everett GA, Madison JT, Marquisee M, Merrill SH, Penswick JR, Zamir A. Structure of a Ribonucleic Acid. Science. 1965; 147:1462–1465. [PubMed: 14263761]

Jia G, Fu Y, He C. Reversible RNA adenosine methylation in biological regulation. Trends Genet. 2013; 29:108–115. [PubMed: 23218460]

Ke S, Alemu EA, Mertens C, Gantman EC, Fak JJ, Mele A, Haripal B, Zucker-Scharff I, Moore MJ, Park CY, et al. A majority of m6A residues are in the last exons, allowing the potential for 3′ UTR regulation. Genes Dev. 2015; 29:2037–2053. [PubMed: 26404942]

Ke S, Pandya-jones A, Saito Y, Fak JJ, Vågbø CB, Geula S, Hanna JH, Black DL Jr, JED, Darnell RB. m 6 A mRNA modifications are deposited in nascent pre-mRNA and are not required for splicing but do specify cytoplasmic turnover. 2017:990–1006.

Kelley DR, Hendrickson DG, Tenen D, Rinn JL. Transposable elements modulate human RNA abundance and splicing via specific RNA-protein interactions. Genome Biol. 2014; 15:537. [PubMed: 25572935]

Langmead B, Salzberg SL. Fast gapped-read alignment with Bowtie 2. Nat Methods. 2012; 9:357–359. [PubMed: 22388286]

Lasda E, Parker R. Circular RNAs Co-Precipitate with Extracellular Vesicles: A Possible Mechanism for circRNA Clearance. PLoS One. 2016; 11:1–11.

Legnini I, Di Timoteo G, Rossi F, Morlando M, Briganti F, Sthandier O, Fatica A, Santini T, Andronache A, Wade M, et al. Circ-ZNF609 Is a Circular RNA that Can Be Translated and Functions in Myogenesis. Mol Cell. 2017; 66:22–37. e9. [PubMed: 28344082]

Liang D, Wilusz JE. Short intronic repeat sequences facilitate circular RNA production. Genes Dev. 2014

Lichinchi G, Gao S, Saletore Y, Gonzalez GM, Bansal V, Wang Yinsheng, Mason CE, Rana TM. Dynamics of the human and viral m6A RNA methylomes during HIV-1 infection of T cells. Nat Microbiol. 2006; 1:2016.

Lin Y, Protter DSW, Rosen MK, Parker R. Formation and Maturation of Phase-Separated Liquid Droplets by RNA-Binding Proteins. Mol Cell. 2015; 60:208–219. [PubMed: 26412307]

Linder B, Grozhik AV, Olarerin-George AO, Meydan C, Mason CE, Jaffrey SR. Single-nucleotide-resolution mapping of m6A and m6Am throughout the transcriptome. Nat Methods. 2015; 12:767–772. [PubMed: 26121403]

Liu J, Yue Y, Han D, Wang X, Fu Y, Zhang L, Jia G, Yu M, Lu Z, Deng X, et al. A METTL3-METTL14 complex mediates mammalian nuclear RNA N6-adenosine methylation. Nat Chem Biol. 2014; 10:93–95. [PubMed: 24316715]

Liu N, Dai Q, Zheng G, He C, Parisien M, Pan T. N(6)-methyladenosine-dependent RNA structural switches regulate RNA-protein interactions. Nature. 2015; 518:560–564. [PubMed: 25719671]

Marzahn MR, Marada S, Lee J, Nourse A, Kenrick S, Zhao H, Ben-Nissan G, Kolaitis RM, Peters JL, Pounds S, et al. Higher-order oligomerization promotes localization of SPOP to liquid nuclear speckles. EMBO J. 2016; 35:1–22. [PubMed: 26567170]

Memczak S, Jens M, Elefsinioti A, Torti F, Krueger J, Rybak A, Maier L, Mackowiak SD, Gregersen LH, Munschauer M, et al. Circular RNAs are a large class of animal RNAs with regulatory potency. Nature. 2013; 495:333–338. [PubMed: 23446348]

Meyer KD, Saletore Y, Zumbo P, Elemento O, Mason CE, Jaffrey SR. Comprehensive Analysis of mRNA Methylation Reveals Enrichment in 3′ UTRs and near Stop Codons. Cell. 2012; 149:1635–1646. [PubMed: 22608085]

Mishima E, Jinno D, Akiyama Y, Itoh K, Nankumo S, Shima H, Kikuchi K, Takeuchi Y, Elkordy A, Suzuki T, et al. Immuno-northern blotting: Detection of RNA modifications by using antibodies against modified nucleosides. PLoS One. 2015; 10:1–17.

Molinie B, Wang J, Lim KS, Hillebrand R, Lu Z, Van Wittenberghe N, Howard BD, Daneshvar K, Mullen AC, Dedon P, et al. m6A-LAIC-seq reveals the census and complexity of the m6A epitranscriptome. Nat Methods. 2016; 13:692–698. [PubMed: 27376769]

Nigro JM, Cho KR, Fearon ER, Kern SE, Ruppert JM, Oliner JD, Kinzler KW, Vogelstein B. Scrambled exons. Cell. 1991; 64:607–613. [PubMed: 1991322]

Ozanick S, Krecic A, Andersland J, Anderson JT. The bipartite structure of the tRNA m1A58 methyltransferase from S. cerevisiae is conserved in humans. RNA. 2005; 11:1281–1290. [PubMed: 16043508]

Pamudurti NR, Bartok O, Jens M, Ashwal-Fluss R, Stottmeister C, Ruhe L, Hanan M, Wyler E, Perez-Hernandez D, Ramberger E, et al. Translation of CircRNAs. Mol Cell. 2017; 66:9–21. e7. [PubMed: 28344080]

Ping XL, Sun BF, Wang L, Xiao W, Yang X, Wang WJ, Adhikari S, Shi Y, Lv Y, Chen YS, et al. Mammalian WTAP is a regulatory subunit of the RNA N6-methyladenosine methyltransferase. Cell Res. 2014; 24:177–189. [PubMed: 24407421]

Polioudakis D, Abell NS, Iyer VR. miR-503 represses human cell proliferation and directly targets the oncogene DDHD2 by non-canonical target pairing. BMC Genomics. 2015; 16:40. [PubMed: 25653011]

Salzman J, Gawad C, Wang PL, Lacayo N, Brown PO. Circular RNAs are the predominant transcript isoform from hundreds of human genes in diverse cell types. PLoS One. 2012; 7:e30733. [PubMed: 22319583]

Schwartz S, Agarwala SD, Mumbach MR, Jovanovic M, Mertins P, Shishkin A, Tabach Y, Mikkelsen TS, Satija R, Ruvkun G, et al. High-resolution mapping reveals a conserved, widespread, dynamic mRNA methylation program in yeast meiosis. Cell. 2013; 155:1409–1421. [PubMed: 24269006]

Shang X, Li G, Liu H, Li T, Liu J, Zhao Q, Wang C. Comprehensive Circular RNA Profiling Reveals That hsa_circ_0005075, a New Circular RNA Biomarker, Is Involved in Hepatocellular Crcinoma Development. Medicine (Baltimore). 2016; 95:e3811. [PubMed: 27258521]

Sigova AA, Mullen AC, Molinie B, Gupta S, Orlando DA, Guenther MG, Almada AE, Lin C, Sharp PA, Giallourakis CC, et al. Divergent transcription of long noncoding RNA/mRNA gene pairs in embryonic stem cells. Proc Natl Acad Sci U S A. 2013; 110:2876–2881. [PubMed: 23382218]

Spitale RC, Flynn Ra, Zhang QC, Crisalli P, Lee B, Jung JW, Kuchelmeister HY, Batista PJ, Torre Ea, Kool ET, et al. Structural imprints in vivo decode RNA regulatory mechanisms. Nature. 2015; 519:486–490. [PubMed: 25799993]

Squires JE, Patel HR, Nousch M, Sibbritt T, Humphreys DT, Parker BJ, Suter CM, Preiss T. Widespread occurrence of 5-methylcytosine in human coding and non-coding RNA. Nucleic Acids Res. 2012; 40:5023–5033. [PubMed: 22344696]

Staehelin M. The primary structure of transfer ribonucleic acid. Experientia. 1971; 27:1–11. [PubMed: 4927151]

Suzuki H, Zuo Y, Wang J, Zhang MQ, Malhotra A, Mayeda A. Characterization of RNase R-digested cellular RNA source that consists of lariat and circular RNAs from pre-mRNA splicing. Nucleic Acids Res. 2006; 34:e63. [PubMed: 16682442]

Wang Y, Wang Z. Efficient backsplicing produces translatable circular mRNAs. RNA. 2015; 21:172–179. [PubMed: 25449546]

Wang P, Doxtader KA, Nam Y. Structural Basis for Cooperative Function of Mettl3 and Mettl14 Methyltransferases. Mol Cell. 2016a; 63:306–317. [PubMed: 27373337]

Wang X, Lu Z, Gomez A, Hon GC, Yue Y, Han D, Fu Y, Parisien M, Dai Q, Jia G, et al. N6-methyladenosine-dependent regulation of messenger RNA stability. Nature. 2014; 505:117–120. [PubMed: 24284625]

Wang X, Zhao BS, Roundtree IA, Lu Z, Han D, Ma H, Weng X, Chen K, Shi H, He C. N6-methyladenosine Modulates Messenger RNA Translation Efficiency. Cell. 2015; 161:1388–1399. [PubMed: 26046440]

Wang X, Feng J, Xue Y, Guan Z, Zhang D, Liu Z, Gong Z, Wang Q, Huang J, Tang C, et al. Structural basis of N6-adenosine methylation by the METTL3–METTL14 complex. Nature. 2016b; 534:1–15.

Xiao W, Adhikari S, Dahal U, Chen YS, Hao YJ, Sun BF, Sun HY, Li A, Ping XL, Lai WY, et al. Nuclear m6A Reader YTHDC1 Regulates mRNA Splicing. Mol Cell. 2016; 61:507–519. [PubMed: 26876937]

Xuan L, Qu L, Zhou H, Wang P, Yu H, Wu T, Wang X, Li Q, Tian L, Liu M, et al. Circular RNA: a novel biomarker for progressive laryngeal cancer. Am J Transl Res. 2016; 8:932–939. [PubMed: 27158380]

Yang Y, Fan X, Mao M, Song X, Wu P, Zhang Y, Jin Y, Yang Y, Chen L, Wang Y, et al. Extensive translation of circular RNAs driven by N6-methyladenosine. Cell Res. 2017:1–16. [PubMed: 28057935]

Zhang H, Elbaum-Garfinkle S, Langdon EM, Taylor N, Occhipinti P, Bridges AA, Brangwynne CP, Gladfelter AS. RNA Controls PolyQ Protein Phase Transitions. Mol Cell. 2015; 60:220–230. [PubMed: 26474065]

Zhang XO, Wang HB, Zhang Y, Lu X, Chen LL, Yang L. Complementary Sequence-Mediated Exon Circularization. Cell. 2014; 159:1–14.

Zhang Y, Zhang XO, Chen T, Xiang JF, Yin QF, Xing YH, Zhu S, Yang L, Chen LL. Circular Intronic Long Noncoding RNAs. Mol Cell. 2013; 51:792–806. [PubMed: 24035497]

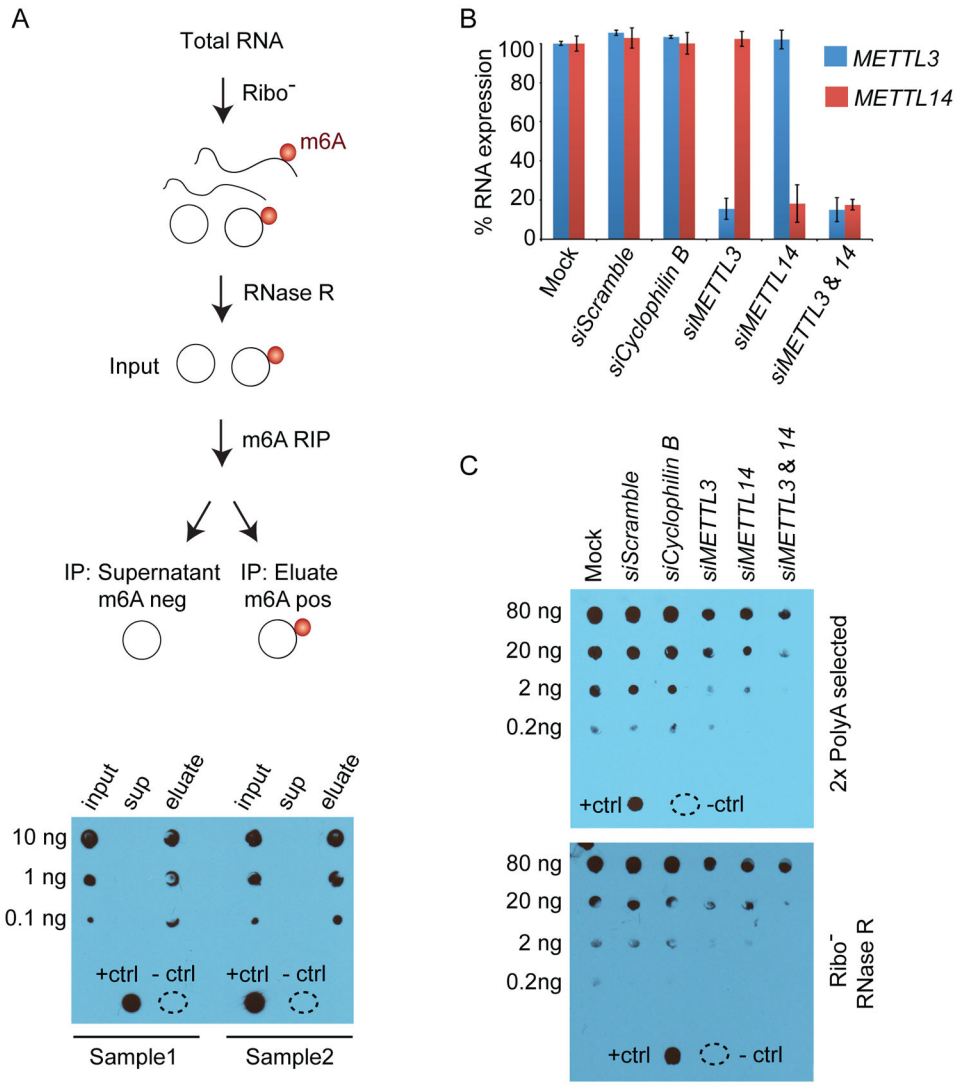

Figure 1. RNase R resistant RNA species are m^{6}A-modified

(A) The diagram describes how total RNA from hESCs was processed. Dot blots for m^{6}A were performed for the indicated amount of RNA. RNA from input (after rRNA-depletion and RNase R treatment), supernatant (sup) and eluate were probed to detect the m^{6}A modification for two replicates (Sample 1 and Sample 2). A positive control (+ctrl) and negative control (−ctrl) containing water are at the bottom of the blot. **(B)** 293T cells were transfected with siRNAs to deplete *METTL3* and *METTL14* as well as negative controls without siRNA (mock), with scrambled siRNA, and with siRNAs that deplete *Cyclophilin B*. Expression of *METTL3* (blue) and *METTL14* (red) was normalized to mock transfection. Error bars represent standard deviation. **(C)** Two rounds of polyadenylated RNA selection (**top**) were performed for each condition in (B). Decreasing amounts of RNA from each condition were probed to detect the m^{6}A. Controls were performed as in (A). Total RNA was isolated from each condition in (B). RNA was rRNA-depleted and treated with RNase R to digest linear RNA (Ribo- RNase R). Decreasing amounts of RNA from each condition were probed to detect m^{6}A in the fraction of RNAs enriched for circRNAs (**bottom**).

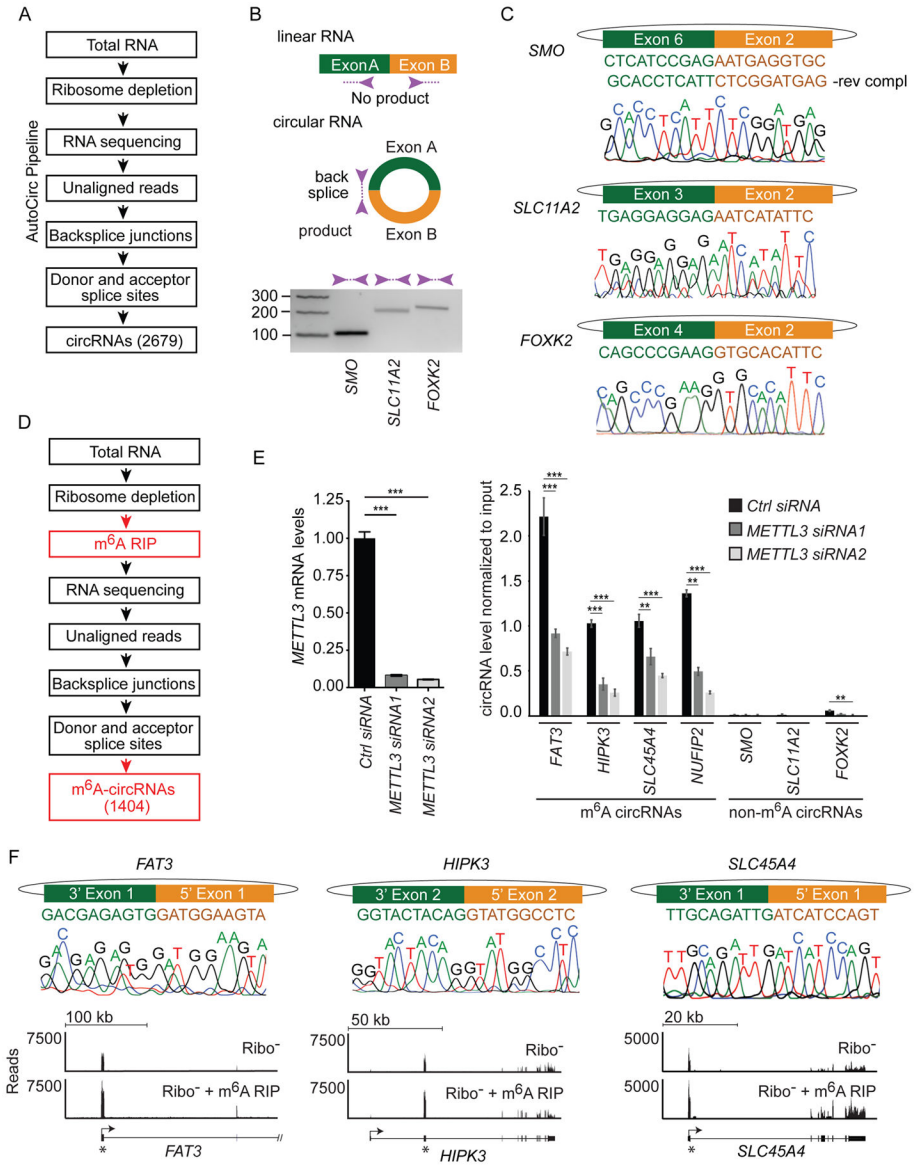

Figure 2. A customized pipeline to identify circRNAs and m^{6}A-modifiied circRNAs

(A) AutoCirc pipeline to detect circRNAs from RNA-seq data. **(B)** RT-PCR validation of identified circRNAs. Divergent primers (purple arrows) only amplify across back splice junctions created in circRNAs. PCR was performed on total RNA after rRNA-depletion. Amplicon size is indicated on the left of the gel. **(C)** Sanger sequencing validation of circRNAs. The exons involved in the back splice junction and the predicted sequence are shown at the top for each transcript. Sanger sequencing results across each back splice junction is shown below each gene. **(D)** Application of AutoCirc to define m^{6}A-circRNAs with new steps in red. **(E)** *METTL3* expression was quantified by qRT-PCR in hESCs transfected with Control (Ctrl) siRNA and two siRNAs depleting *METTL3* (left). Error bars represent standard deviation. *** indicates p<0.001. Detection of back splice junctions for circRNAs encoded by the indicated genes after m^{6}A RIP is shown in the right. Black boxes represent hESCs transfected with Ctrl siRNA and the two shades of gray indicate hESCs

transfected with siRNAs targeting *METTL3* (right). m^6A-circRNAs and non-m^6A-circRNAs are indicated. Error bars represent standard deviation. *** indicates $p< 0.0001$ and ** indicates $p< 0.001$. Amplification of each back splice was tested for each sample prior to m^6A-RIP (Figure S2G). **(F)** Sanger sequencing across the back splice forming m^6A-circRNAs. The exons involved and predicted sequence is show at the top for each transcript. Sanger sequencing results across each back splice junction are shown in the middle. RNA-seq tracks are shown at the bottom for total RNA following rRNA depletion (Ribo-) and after rRNA depletion followed by m^6A RIP. The gene structure is shown below the tracks. Arrows indicate the direction of transcription and asterisks indicate the exons that are circularized.

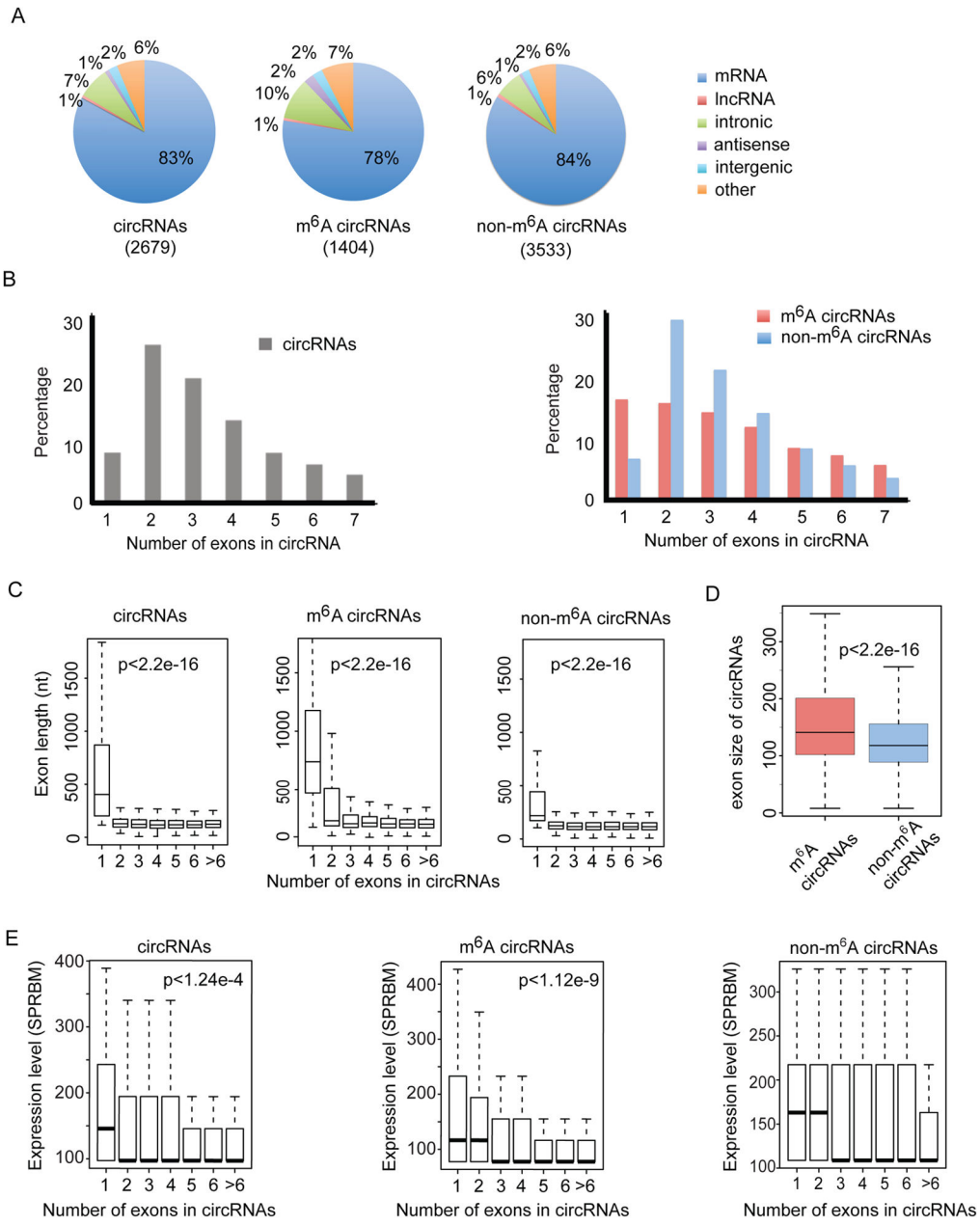

Figure 3. CircRNAs are frequently methylated in human embryonic stem cells

(A) Genomic distribution of total circRNAs (input, left), m^{6}A-circRNAs (eluate, center), and non-m^{6}A-circRNAs (supernatant, right). The total number of circRNAs identified in each condition is shown in parenthesis. **(B)** The percentage of circRNAs (y-axis) was calculated based on the number of exons each circRNA spans (x-axis) for input circRNAs (left), m^{6}A-circRNAs (red, right panel) and non-m^{6}A-circRNAs (blue, right panel). The number of exons up to seven is displayed. **(C)** The distributions of exon length (y-axis) for input circRNAs (left), m^{6}A-circRNAs (middle) and non-m^{6}A-circRNAs (right) are plotted based on the number of exons spanned by each circRNA (x-axis). **(D)** Comparison of exon size of m^{6}A-circRNAs and non-m^{6}A-circRNAs. **(E)** Expression levels (y-axis) for input circRNAs,

m^{6}A-circRNAs, and non-m^{6}A-circRNAs are plotted based on the number of exons spanned by each circRNA (x-axis). P values indicate that single exon circRNAs are more abundant than circRNAs composed of more than one exon.

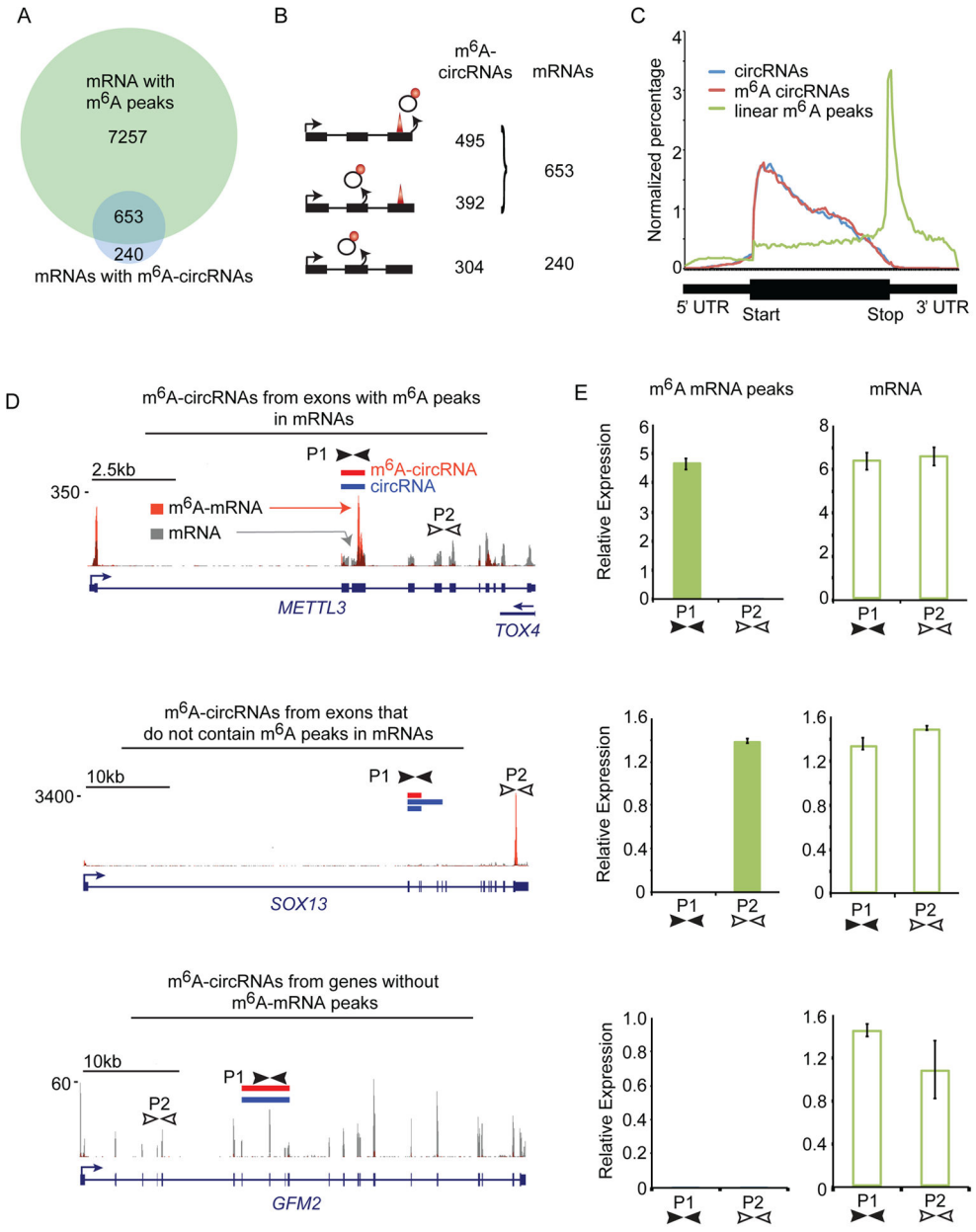

Figure 4. m^{6}A-circRNAs are often methylated in regions where m^{6}A-mRNAs are not methylated

(A) Venn diagram showing the overlap between genes encoding m^{6}A-circRNAs and genes encoding m^{6}A-mRNAs. The total number of genes in each category is shown. **(B)** Distribution of m^{6}A-modified exons between circRNAs and mRNAs: m^{6}A sites in the same exons (top); m^{6}A sites are on different exons from the same parent gene (middle); m^{6}A sites are only present on circRNAs (bottom). The total number of m^{6}A-circRNAs and mRNAs in each category are shown. **(C)** Distribution of exons encoding m^{6}A-circRNAs (red) and total circRNAs (blue) across genes compared to the distribution of m^{6}A peaks in mRNAs across genes (green). The region from the transcription start site (TSS) to the start of the coding sequence (start) represents the 5′ UTR and the region from the end of the coding sequence (Stop) to the 3′ end represents the 3′ UTR. **(D)** Examples of genes described in (B). Red

bars indicate m^6A-circRNAs detected by sequencing. Blue bars represent circRNAs identified by sequencing. Tracks below the circRNAs represent m^6A peaks from polyadenylated mRNAs before and after m^6A RIP (Batista et al., 2014). Gray peaks represent mRNA background levels, and orange peaks represent sites of m^6A modification in mRNAs. The locations of primer sets for each transcript are indicated by black and white arrows (P1 and P2). (P1, P2) **(E)** qRT-PCR was performed on cDNA following polyA selection and m^6A RIP (m^6A mRNA peaks) and following polyA selection alone (mRNA) for the genes in (D).

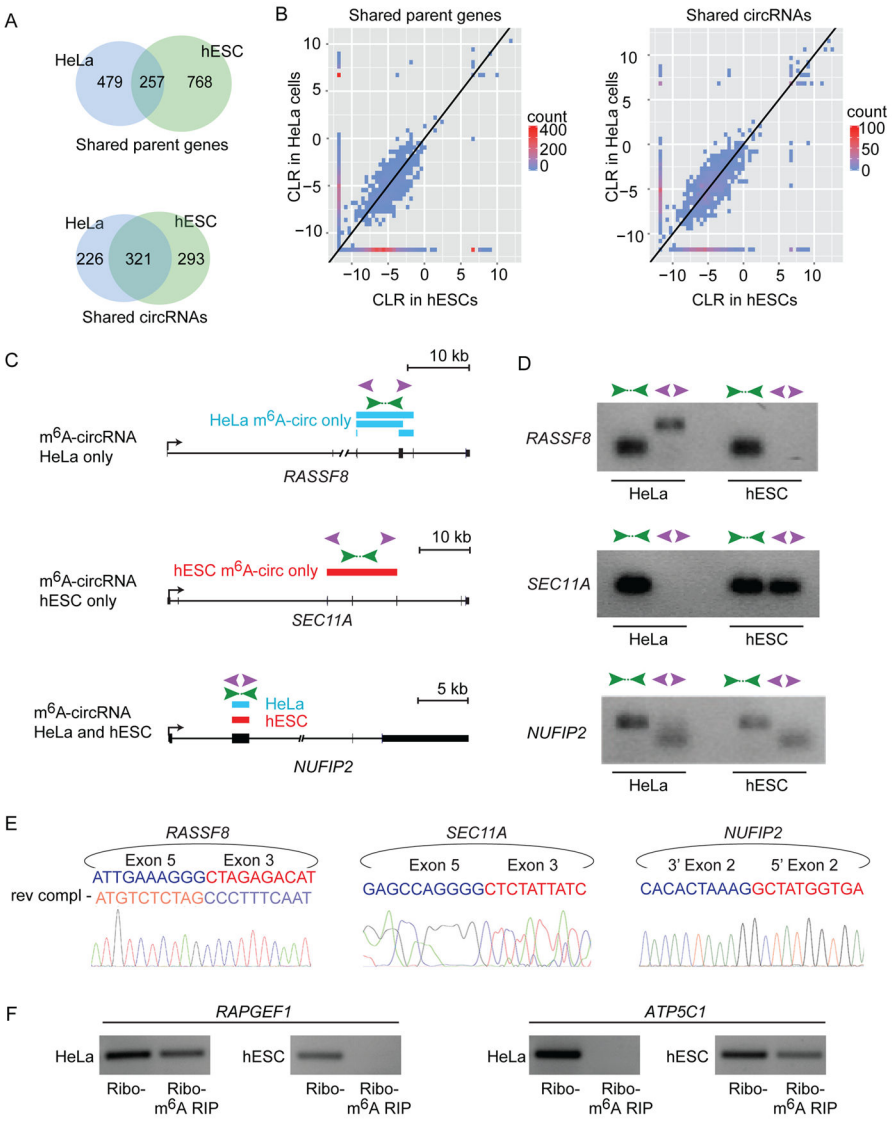

Figure 5. m^{6}A-circRNAs show cell-type-specific patterns of expression

(A) Venn diagram shows the overlap of m^{6}A-circRNAs encoded by genes expressed in HeLa cells and hESCs with RPKM > 1 in both cell types (Shared parent genes, top). The overlap between m^{6}A-circRNAs among circRNAs that are detected in both HeLa cells and hESCs is shown below (Shared circRNAs). **(B)** Two-dimensional histograms comparing the expression levels of m^{6}A-circRNAs in HeLa cells and hESCs. m^{6}A-circRNAs in the left panel are encoded by genes that are expressed in both HeLa cells and hESCs (Shared parent genes). m^{6}A-circRNAs in the right panel show m^{6}A-circRNA levels for all circRNAs common in both HeLa cells and hESCs (Shared circRNAs). CircRNA counts are indicated on the scale to the right of each plot. m^{6}A-circRNA expression levels are calculated by the circular-to-linear ratio (CLR). **(C)** Examples of m^{6}A-circRNAs that that are unique to HeLa cells (top), unique to hESCs (middle), and common between HeLa cells and hESCs (bottom). Blue rectangles indicated m^{6}A-circRNAs identified in HeLa cells, and red rectangles indicate m^{6}A-circRNAs identified in hESCs. Green arrows indicate the location

of primers that amplify across forward splice junctions and purple arrows indicate primers that amplify across back splices. **(D)** RT-PCR was performed on RNA prepared following rRNA depletion in HeLa cells and hESC cells, respectively. **(E)** Sanger sequencing was performed on PCR products generated by amplifying across back splice junctions for the indicated genes. Sequencing across the junction is shown in sense for *SEC11A* and *NUFIP2* and antisense (rev compl) for *RASSF8*. **(F)** RT-PCR was performed on rRNA-depleted RNA (Ribo-) and after m^6A RIP (Ribo-, m^6A RIP) in HeLa cells and hESCs, respectively.

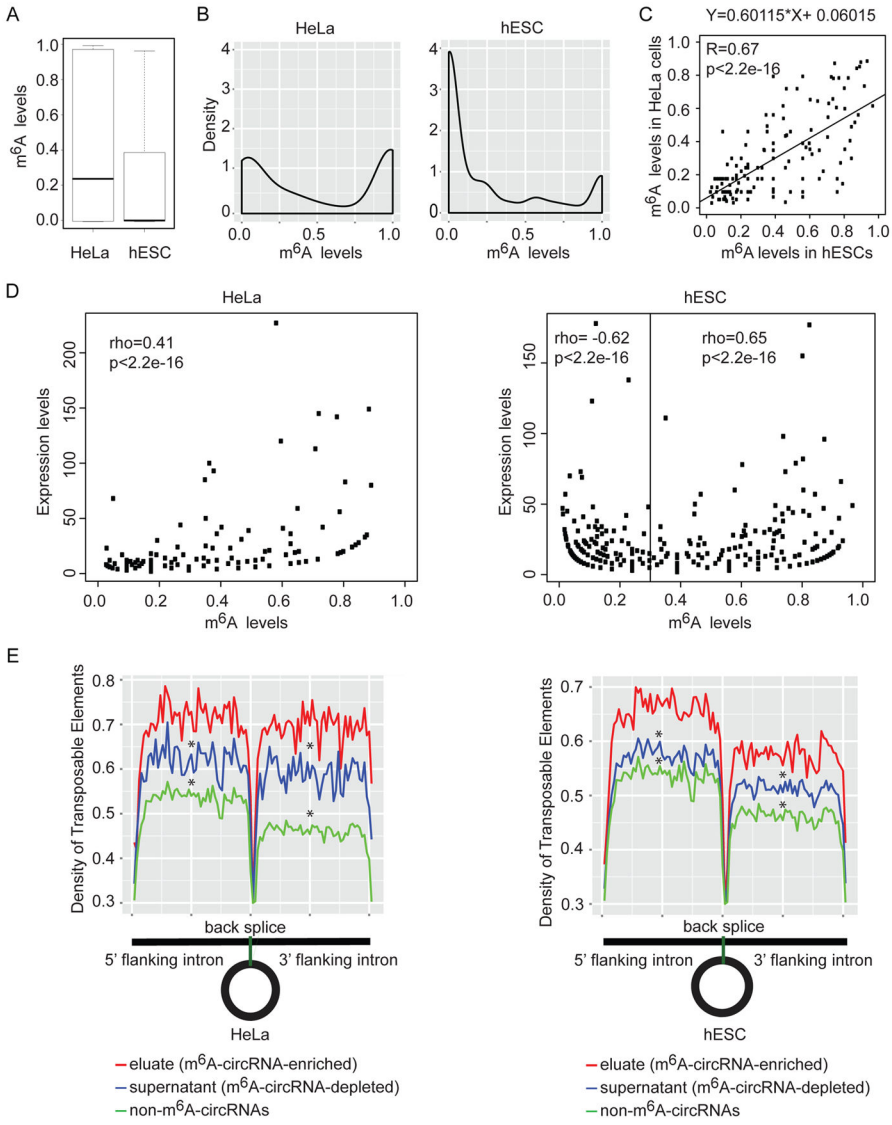

Figure 6. m^{6}A levels

(A) Comparison of m^{6}A levels in circRNAs in HeLa cells and hESCs with at least 2 reads supporting the back splice junctions in eluate and supernatant data. **(B)** Density distributions of m^{6}A levels in circRNAs using the same criteria as in (B). **(C)** Scatter plot showing the linear correlations of m^{6}A levels among the m^{6}A-circRNAs identified in both HeLa cells and hESCs. The linear regression fit equation is indicated in the top. The Pearson correlation coefficient and p-value are indicated at the top left corner. **(D)** The relationship between expression levels of circRNAs and m^{6}A levels of circRNAs in HeLA cells (left) and hESCs (right). Expression levels are represented by back splice read counts of circRNAs in eluate and supernatant data. **(E)** Density distribution of transposable elements (TEs) flanking circRNAs. Eluate (red) contains circRNAs identified by m^{6}A RIP (m^{6}A-circRNA-enriched). Supernatant (blue) contains circRNAs not precipitated by m^{6}A RIP (m^{6}A-circRNA-depleted). Non-m^{6}A-circRNAs (green) contains circRNAs identified in either HeLa or hESC

supernatant that were not detected in either HeLa or hESC eluates. * indicates p<2.2e-16 compared to eluate.

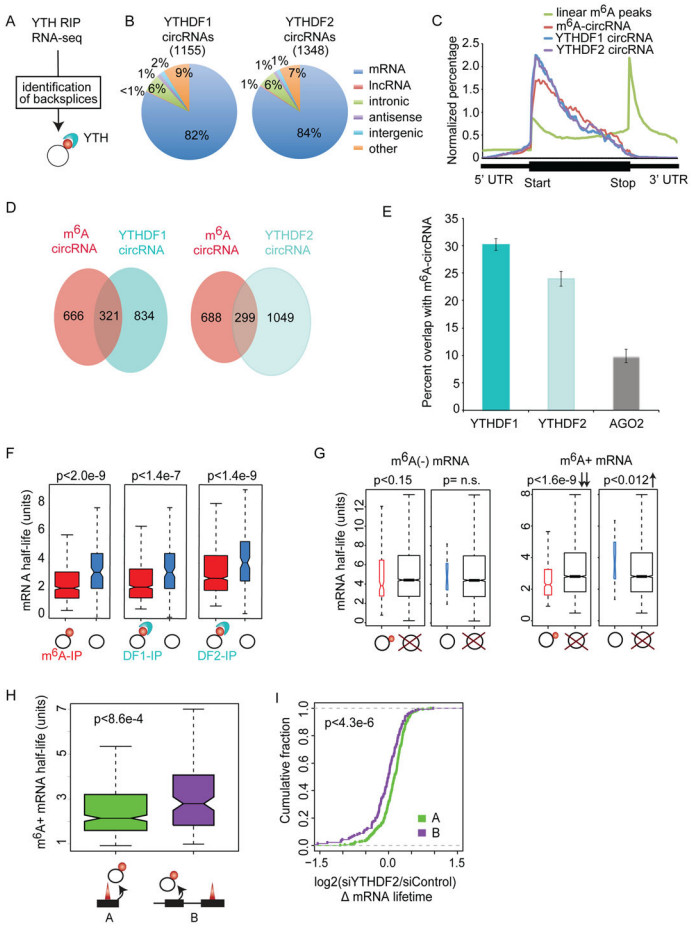

Figure 7. m^{6}A-circRNAs bind YTHDF1 and YTHDF2 and identify transcripts with shorter half-lives

(A) Data from YTHDF1 and YTHDF2 RIP-seq (Wang et al., 2014, 2015) were used to identify m^{6}A-circRNAs in HeLa cells. **(B)** The genomic distribution of circRNAs bound by YTHDF1 and YTHDF2 are shown. The number of circRNAs associated with each protein is indicated in parenthesis. **(C)** The distribution of exons encoding circRNAs associated with YTHDF1 (blue) and YTHDF2 (purple) compared to exons encoding m^{6}A-circRNAs (red) and the distribution of m^{6}A peaks across mRNAs (green) is shown. **(D)** Venn diagram shows the overlap between m^{6}A-circRNAs identified in HeLa cells and m^{6}A-circRNAs bound by YTHDF1 (left) and YTHDF2 (right). **(E)** The percentage of m^{6}A-circRNAs identified by m^{6}A RIP in HeLa cells and bound by YTHDF1, YTHDF2, or AGO2 are shown. Error bars represent standard deviation. **(F)** mRNA half-life for parent genes that encode m^{6}A-circRNAs (left), YTHDF1-bound (DF1-IP) circRNAs (middle), or YTHDF2-bound (DF2-IP) circRNAs (right). Black rings represent circRNAs, red circles indicate m^{6}A modification, and light blue structures represent YTH proteins. **(G)** The mRNA half-life for m^{6}A negative (m^{6}A (−) mRNA) (left) and m^{6}A positive mRNAs (m^{6}A (+) mRNA) (right) whose parent genes encode m^{6}A-circRNAs (black ring with red circle attached), circRNAs without m^{6}A (black ring), or no circRNAs (black ring with red “X”). p values are indicated above each plot. **(H)** The half-life of m^{6}A-mRNAs whose parent genes also encode m^{6}A-

circRNAs from the same exon(s) where an m^6A peak is found in mRNA (labeled A) is compared to the half-life of m^6A-mRNA whose parent gene encodes an m^6A circRNA at exon(s) where no m^6A peak is found in mRNAs (labeled B). **(I)** The change in half-life (log2(siYTHDF2/siControl)) was calculated after depletion of YTHDF2 as described (Wang et al., 2014) for condition A (green) and condition B (purple). The p values were calculated using Wilcoxon-Mann-Whitney test. Figure S6 shows the second replicate.